Westinghouse Non-Proprietary Class 3

WCAP-17202-NP
Revision 0

June 2010

Supplement 4 to BISON Topical Report RPA 90-90-P-A

Westinghouse

WESTINGHOUSE NON-PROPRIETARY CLASS 3

WCAP-17202-NP
Revision 0

Supplement 4 to BISON Topical Report RPA 90-90-P-A

Lena Olsson
BWR Transient Analysis

Henrik Björke
BWR Transient Analysis

June 2010

Reviewer:	Thomas Lindqvist USBWR & Criticality
Prepared by:	Ryan Lenahan* Fuel Engineering Licensing
Approved:	Kris Cummings*, Manager Fuel Engineering Licensing

*Electronically approved records are authenticated in the electronic document management system.

Westinghouse Electric Company LLC
P. O. Box 355
Pittsburgh, PA 15230-0355

© 2010 Westinghouse Electric Company LLC
All Rights Reserved

TABLE OF CONTENTS

1 Introduction 1-1

1.1 BACKGROUND AND REPORT OBJECTIVE 1-1
1.2 SUMMARY AND CONCLUSIONS 1-2
1.3 SCOPE OF REVIEW 1-2
2 Resolution of SER Restriction 2-1

2.1 PURPOSE 2-1
2.2 BISON RECIRCULATION PUMP MODEL DESCRIPTION 2-1
2.2.1 RUNNING PUMP 2-1
2.2.2 STOPPED PUMP 2-2
2.2.3 PARALLEL PUMPS 2-2
2.3 VALIDATION OF MODEL 2-3
2.3.1 REACTOR INTERNAL PUMP TRIP TEST 2-3
2.3.2 GENERATOR LOAD REJECTION TEST 2-5
3 Additional Qualification of BISON models 3-1

3.1 ADVANCED CONTROL ROD HYDRAULIC INSERTION MODEL 3-1
3.1.1 PURPOSE 3-1
3.1.2 DESCRIPTION OF MODEL 3-1
3.1.3 VERIFICATION OF MODEL 3-10
3.1.4 VALIDATION OF MODEL 3-12
3.1.5 CONCLUSIONS 3-14
3.2 IMPROVED METHOD FOR CROSS-SECTION COLLAPSING 3-14
3.2.1 PURPOSE 3-14
3.2.2 DESCRIPTION OF THE IMPROVED METHOD 3-14
3.2.3 VALIDATION OF MODEL 3-15
3.2.4 CONCLUSIONS 3-23
3.3 ASYNCHRONOUS PUMP MOTOR 3-24
3.3.1 PURPOSE 3-24
3.3.2 DESCRIPTION OF MODEL 3-24
3.3.3 VALIDATION OF MODEL 3-27
3.4 BISON/SAFIR INTERFACE FOR LEVEL MEASUREMENT 3-28
3.4.1 PURPOSE 3-28
3.4.2 DESCRIPTION OF MODEL 3-28
3.4.3 VALIDATION OF MODEL 3-30
3.5 STEAM DOME WATER SURFACE CONDENSATION MODEL 3-31
3.5.1 PURPOSE 3-31
3.5.2 DESCRIPTION OF MODEL 3-31
3.5.3 VERIFICATION OF MODEL 3-32
3.5.4 VALIDATION OF MODEL 3-33
3.5.5 CONCLUSIONS 3-34
3.6 POST DRYOUT AND REWET MODEL 3-35
3.6.1 PURPOSE 3-35
3.6.2 DESCRIPTION OF MODEL 3-35

3.6.3 VALIDATION OF MODEL 3-39
3.6.4 CONCLUSIONS 3-42
4 References 4-1

LIST OF TABLES

Table 3-1 Control Rod Groups in the [ ][a,c] Scram System 3-13

Table 3-2 Measured and Calculated Control Rod Insertion Times in [ ][a,c] 3-13

Table 3-3 Peach Bottom 2 Main Process Parameters 3-18

Table 3-4 Reactivity Change Caused by a [ ][a,c] Change in Recirculation Flow 3-20

Table 3-5 Defined Impedances in Figure 3-16 3-26

LIST OF FIGURES

Figure 2-1 Reactor Internal Pump flow for a ABWR, after a 3 RIP trip event 2-4

Figure 2-2 Reactor Internal Pump speed for a ABWR, after a 3 RIP trip event 2-4

Figure 2-3 Reactor Internal Pump Trip Speed Comparison 2-5

Figure 3-1 Advanced Control Rod Hydraulic Insertion Model for ABWR 3-3

Figure 3-2 [ ]^{a,c} Control Rod Hydraulic Insertion (SCRAM) Times 3-11

Figure 3-3 [ ]^{a,c} Control Rod Hydraulic Insertion (SCRAM) Times 3-12

Figure 3-4 Comparison of Homogeneous Core Normalized Axial Power Profile 3-16

Figure 3-5 Comparison of Heterogeneous Core Normalized Axial Power Profile 3-17

Figure 3-6 Comparison of Normalized Axial Power Profile with Improved Cross-Section Collapsing Method for TT1 3-18

Figure 3-7 Comparison of Normalized Axial Power Profile with Improved Cross-Section Collapsing Method for TT2 3-19

Figure 3-8 Comparison of Normalized Axial Power Profile with Improved Cross-Section Collapsing Method for TT3 3-19

Figure 3-9 Comparison of APRM for TT1 3-20

Figure 3-10 Comparison of Integrated APRM for TT1 3-21

Figure 3-11 Comparison of APRM for TT2 3-21

Figure 3-12 Comparison of Integrated APRM for TT2 3-22

Figure 3-13 Comparison of APRM for TT3 3-22

Figure 3-14 Comparison of Integrated APRM for TT3 3-23

Figure 3-15 Block Diagram of the BISON Pump Model 3-24

Figure 3-16 Equivalent Scheme For the BISON Model of the Asynchronous Motor 3-25

Figure 3-17 Representative Half Reactor Including the Stream Dryer in BISON 3-29

Figure 3-18 Condensation Model Compared to Test Data 3-32

Figure 3-19 Pressure (Pa) as a Function of Time (seconds) for a Load Rejection With Bypass Transient 3-33

Figure 3-20 Pressure (Pa) as a Function of Time (seconds) for a Main Steamline Isolation Valve Closure Transient 3-34

Figure 3-21 Rewet Quench Velocity as a Function of Temperature Difference 3-38

Figure 3-22 Predicted versus Measured Temperature Increases for [ ]^{a,c} Experiments 3-39

Figure 3-23 Predicted versus Measured Temperature Increases for [ ]a,c Experiments, using conservative method for PCT calculation 3-40

Figure 3-24 Predicted versus measured temperature increases for [ ]a,c 3-40

Figure 3-25 Predicted versus measured temperature increases for [ ]a,c 3-41

Figure 3-26 Predicted versus measured temperature increases for [ ]a,c 3-41

LIST OF ACRONYMS

ABWR	Advanced Boiling Water Reactor
AVZ	Above Vessel Zero
COLA	Combined Construction and Operating License Application
COLR	Core Operating Limits Report
CPR	Critical Power Ratio
EOC2	End of Cycle 2
LRWBP	Load Rejection With Bypass
LTR	Licensing Topical Report
MSIV	Main Steamline Isolation Valve
MSIVC	Main Steamline Isolation Valve Closure
OLMCPR	Operating Limit Minimum Critical Power Ratio
PB2	Peach Bottom Unit 2
PCT	Peak Cladding Temperature
RIP	Reactor Internal Pump
RPV	Reactor Pressure Vessel
SER	Safety Evaluation Report
TCV	Turbine Control Valve
TH	Hydraulic Torque
U.S. NRC	United States Nuclear Regulatory Commission

NOMENCLATURE FOR EQUATIONS

A_1	Inner area for the gas tank-scram valve line
A_3	Inner area of the main line after the water tank
A_{32}	Inner area of branch line to rotary actuator
A_4	Plunge area of the rotary actuator
A_{41}	Effective leakage area in the rotary actuator
A_{rel}	Relative opening area for a scram valve in the water line
A_{w1}	Inner wall area of the gas tank (for heat transfer)
A_{w2}	Heat transfer area in the water tank
C_p	Heat capacity
c_p	Isobaric thermal capacity for nitrogen gas
c_v	Isochore thermal capacity for nitrogen gas
Dh	Hydraulic diameter
Eta	Dynamic viscosity
F	Notation for water
FR	Frictional force in an actuator
g	Gravity constant
G	Notation for steam
G_1	Gas flow between the gas tank and the water tank
G_2	Mass flow water in the main line from the water tank
G_{21}	Mass flow to the extracted actuators
G_{22}	Mass flow to the non extracted actuators
G_3	Mass flow water in the branch line to the rotary actuator

G_{41}	Leakage flow past the plunge in the rotary actuator
h_1	Enthalpy for the gas in the gas tank
h_2	Enthalpy for the gas after the water tank
h_{fg}	Latent heat of vaporization
h_G	Stagnation enthalpy for the gas flow G1
HP_3	Plus height for the water tank
HP_4	Plus height for the rotary actuator
HP_5	Plus height for the water surface in the reactor tank
L_3	Length of the main line after the water tank
L_{32}	Length of a branch line from the main line to rotary actuator (average for the group)
Leid	Leidenfrost
M_{don}	Weight of moving parts (including control rods) for a rotary actuator
M_1	Mass for the gas in the gas tank
M_2	Mass for the gas in the water tank
N_{don}	Number of rotary actuators in the group in question
N_{don1}	Number of extracted rotary actuators in the group
N_{don2}	Number of fully inserted rotary actuators in the group
Pr	Prandtl's number
p_1	Pressure in the gas tank
p_{12}	Pressure in smallest section or the venturi nozzle
p_2	Pressure in the water tank
p_4	Pressure in rotary actuator (under plunger)
p_5	Reactor steam dome pressure
p_{45}	Pressure difference across the plunger in the rotary actuator
p_{br}	Specific breaking power from the hydraulic brake
q_1	Heat flow from the gas tank wall to the gas in the tank
q_2	Heat flow from the pipe walls and water to the gas in the water tank
r	Radius
R	The individual gas constant for nitrogen gas
Re	Reynold's number
Sat	Saturation
T	Temperature
T_1	Gas temperature in the gas tank
T_2	Gas temperature in the water tank
T_{10}	Initial temperature for the gas in the gas tank. The tank walls are presumed to maintain this temperature
T_{20}	Initial value for T2. Pipe and tank walls are presumed to stay at this temperature
T_G	Stagnation temperature for the gas flowing through the reactor scram valve
t_{open}	Time to when the scram valve starts to open (cone leaves its seat)
t_v	Effective valve opening time for the scram valve
u_1	Inner energy for the gas in the gas tank
u_2	Inner energy in the water tank
V_1	Volume of the gas tank
V_2	Volume of the gas in the water tank including feed line
V_3	Volume of the water in the water tank
V_{23}	The total volume of the water tank

w	Speed of the actuators moving parts
Wall	Cladding surface
x	Coordinate for rotary actuator position
X	Steam quality
α	Factor to account for the impact of water when accelerating the rotary actuator's moving parts
α_1	Effective thermal exchange constant between the gas in the gas tank and the walls of the tank
α_2	Effective heat exchange constant between the gas in the water tank and pipe and tank walls as well as water
α_{void}	void reactivity feedback of a recirculation flow change
ε	Emissivity
λ	Thermal conductivity
ξ_1	Drag coefficient for the gas tank-scram valve
ξ_3	Drag coefficient for the main line after the water tank
ξ_{32}	Drag coefficient for the branch line to a rotary actuator (average within a group)
κ	Isentropic exponent for nitrogen gas
ρ	Density
ρ_1	Density of the gas in the gas tank
ρ_2	Density for the water in the water tank
ρ_g	Density for gas
ρ_s	Density of the material in the moving parts of the rotary actuator
σ	Water surface tension

1 INTRODUCTION

1.1 BACKGROUND AND REPORT OBJECTIVE

The Westinghouse transient analysis code BISON is described in Licensing Topical Reports (LTRs) RPA 90-90-P-A "BISON – A One Dimensional Dynamic Analysis Code for Boiling Water Reactors" (Reference 1), CENPD-292-P-A "BISON – One Dimensional Dynamic Analysis Code for Boiling Water Reactors: Supplement 1 to Code Description and Qualification" (Reference 2), WCAP-16606-P-A "Supplement 2 to BISON Topical Report RPA 90-90 P-A" (Reference 3), and Westinghouse Report WCAP-17079-P, "Supplement 3 to BISON Topical Report RPA 90-90-P-A SAFIR Control System Simulator" (Reference 4). The BISON code is applicable to BWR/2-6 and ABWR.

RPA 90-90-P-A describes the BISON transient code and the code qualification for BWR transient analyses and was approved for use in license applications by the U.S. NRC in 1989. CENPD-292-P-A was submitted to introduce changes and upgrades to the methods in order to address some of the Safety Evaluation Report (SER) restrictions on the original LTR and was approved in 1995. WCAP-16606-P-A was submitted to introduce changes related to ATWS calculations and to increase the range of verification to higher pressures and steam qualities, and it was approved in 2007. WCAP-17079-P is under review by the U.S. NRC and was submitted to extend the code applicability to address SER restriction 6 in RPA 90-90-P-A regarding modelling of control systems.

The main purpose of this LTR, which will be the fourth supplement to the BISON LTR, is to address restriction 2 in RPA 90-90-P-A in addition to including new models in the BISON code required to extend the code capability to include a first time transient analysis application. In addition to extending the code capability, these models provide a more robust analysis for the current application of BISON.

The BISON code is used for reload applications and other plant changes which only require limiting transients to be evaluated. Westinghouse intends to expand the scope of BISON to include all limiting and non-limiting transients required for a first time transient analysis application. The additional methods and models described in this topical extend the qualification of BISON to address these additional phenomena necessary for a full scope analysis. The new methods and models, that are intended to be used for all transients including limiting transients, are:

The Advanced Control Rod Hydraulic Insertion Model

This model is used to model the ABWR plant scram velocity versus time instead of using user defined tables of control rod position versus time. This allows a more realistic but conservative modelling of control rod insertion. The model application is limited to the ABWR only.

Improved Method for Cross-Section Collapsing

An improved method for nuclear cross-section collapsing is introduced. This model was developed after the approval of the nodal code POLCA7 Reference 7. This new collapsing model uses input from POLCA7 to produce more accurate results in 1D. The method also has a significant advantage regarding user-friendliness. This model is intended for BWR/2-6 and the ABWR.

Asynchronous Pump Motor Model

The asynchronous pump motor model is intended to be used with SAFIR generated control systems to model recirculation pumps. This model is intended for BWR/2-6 and the ABWR.

Steam Dome Water Surface Condensation Model

This model is used to capture phenomena related to steam condensation on the water surface of the bulk water when subcooled water interacts with a steam environment. [

]^{a,c} This model is intended for BWR/2-6 and the ABWR.

Post Dryout and Rewet Model

For events that require the radiological consequences to be evaluated the post dryout and rewet model determines the Peak Cladding Temperature (PCT). This is required to determine the number of fuel rods experiencing cladding failure during the transient. This model is intended for BWR/2-6 and the ABWR.

1.2 SUMMARY AND CONCLUSIONS

Based on the information provided in this report, it is concluded that the BISON code can be used for licensing transient analysis of all transients included in a first core transient analysis application to demonstrate compliance to the applicable regulatory requirements in the General Design Criteria in 10CFR50, Appendix A.

1.3 SCOPE OF REVIEW

Based on the information included in this report, Westinghouse requests NRC review and approval for:

- Method to address SER restriction 2 from BISON, RPA 90-90-P-A (Reference 1)
- Approval of the following BISON models for licensing applications:
    - Advanced control rod hydraulic insertion model
    - New method for cross-section collapsing
    - Asynchronous pump motor
    - BISON/SAFIR interface for level measurement
    - Steam dome water surface condensation model
    - Post dryout and rewet model

2 RESOLUTION OF SER RESTRICTION

SER restriction 2 in the BISON LTR RPA 90-90-P-A (Reference 1), states: "We require justification for use of the recirculation pump model when transients are in other than the first quadrant of the Karman-Knapp diagram." It is necessary to address this restriction to model the ABWR internal recirculation pumps.

A trip of a limited number (not all) recirculation pumps can be included as a part of the reactor protection system. In the tripped pumps the flow can become reversed. A description of how reverse flow through the recirculation pump is modelled in BISON is provided in Section 2.2. The start-up tests of Hamaoka Unit 5 will be used for validation of the BISON model (Reference 5). The tests include trips of the recirculation pumps while other pumps are running, giving a reversed flow in the tripped pumps. The total recirculation flow is the sum of the pump flows.

2.1 PURPOSE

A transient where recirculation pumps trip can cause the recirculation pumps to operation outside the first quadrant of the Karman-Knapp diagram. To be able to model transients where one or more Reactor Internal Pumps (RIP) trip, and the phenomena of reversed RIP flow, a justification of using the BISON pump model outside the first quadrant in the pump characteristics diagram (running pump) is needed.

2.2 BISON RECIRCULATION PUMP MODEL DESCRIPTION

The asynchronous pump motor model used to drive the pump is described in Section 3.3.

2.2.1 Running Pump

For the first quadrant in the pump characteristics diagram (running pump), the recirculation pump model calculates the pump pressure set up as a function of pump flow and rotational speed. The pump speed may be prescribed by the user or calculated by the model (shown in Reference 1).

The user supplies pump characteristics (Pump head, H, and Hydraulic torque, TH) for a homologous pump model for nominal pump speed. Pump head H and Hydraulic torque TH at arbitrary pump speeds and volume flows are then calculated from nominal speed pump curves using the general formula (shown in Reference 1):

$$f(W(t), N(t)) = (N(t)/N_R)^2 F(W(t)/N(t), N_R) \qquad \text{Equation 2-1}$$

Where t is the time, N(t) is actual pump speed, N_R is the nominal pump speed and F(W, N_R) is the characteristic curve as a function of volume flow W at nominal speed N_R.

2.2.2 Stopped Pump

When the pump speed falls below a certain value (given as an input by the user), the code considers the pump to be stopped. Pump speed is not calculated and the pump is treated as a flow restriction. Two stopped pump cases are considered:

- Wind-milling pump, characterized by zero torque (T=0) and non-zero pump blade rotation (rpm≠0)
- Stationary pump, characterized by non-zero torque (T≠0) and zero pump blade rotation (rpm=0)

Whether the pump is treated as stationary or wind-milling is dependent on the mass flow. For the mass flow in both forward and reverse direction, two values are given as users input:

- Mass flow for which a wind-milling pump will stop (change from wind-milling to stationary)
- Mass flow for which a stationary pump will start wind-milling

2.2.2.1 Wind-Milling Pump

The pump head in SI units (Pa) is obtained from the following equation:

$$dP_{pump} = -\xi_{wind} W_p \left| W_p \right| \qquad \text{Equation 2-2}$$

where W_p is the pump flow (m^3/s) and ξ_{wind} is the user specified loss coefficient for a wind-milling pump. Two values for the loss coefficient are required; one for the forward, and one for the reverse flow direction.

2.2.2.2 Stationary Pump

The pump head in SI units (Pa) is obtained from the following equation:

$$dP_{pump} = -\xi_{stat} W_p \left| W_p \right| \qquad \text{Equation 2-3}$$

where W_p is the pump flow (m^3/s) and ξ_{stat} is the user specified loss coefficient for a stationary pump. Two values for the loss coefficient are required; one for the forward, and one for the reverse flow direction.

2.2.3 Parallel Pumps

BISON allows the specification of different parallel pump groups. Each parallel pump group can be set as running or stopped. The pump head over each pump group has to be the same. [

]a,c

2.3 VALIDATION OF MODEL

Start-up test data from Hamaoka Unit 5 (Reference 5) were used to validate the modelling capability of the BISON pump model outside of the first quadrant of the Karman-Knapp diagram. The start-up tests include trip of recirculation pumps and generator load rejection, which result in a trip of four out of ten recirculation pumps. The tests recorded the results of three/four recirculation pumps tripped and seven/six pumps running giving a reversed flow in the tripped pumps. The total recirculation flow is the sum of the flows through all of the pumps.

2.3.1 Reactor Internal Pump Trip Test

The BISON pump model has been validated with a reactor internal pump trip test, performed at the Hamaoka Unit 5 reactor. Three out of ten RIPs were tripped and the reactor response was measured. Due to the pressure difference across the tripped pumps and the running pumps being the same (positive), the flow through all the pumps changes such that the flow through the stopped pumps becomes negative. This transient is simulated using the BISON code with the recirculation pump model described in Section 2.2 (three RIPs stopped and seven in operation). The BISON simulation is compared to experimental data as shown in Figure 1 and Figure 2 in Appendix A.

As can be observed from the results, the calculated total core flow is in very good agreement with the test data, which proves the validity of the recirculation pump model implementation in the BISON code. In Figure 2-1 and Figure 2-3 individual recirculation pump data from BISON is shown for a three RIP trip analyzed for an ABWR. The RIP flow, for one running pump and one pump that is tripped is shown in Figure 2-1. and the corresponding recirculation pump speed is shown in Figure 2-2. For Hamaoka 5 reactor internal pump trip test, the relative RIP speed is shown for a tripped pump in Figure 2-3. [

]^{a,c}

a,c

[ ]

Figure 2-1 Reactor Internal Pump flow for a ABWR, after a 3 RIP trip event

a,c

[ ]

Figure 2-2 Reactor Internal Pump speed for a ABWR, after a 3 RIP trip event

a,b,c

Figure 2-3 Reactor Internal Pump Trip Speed Comparison

2.3.2 Generator Load Rejection Test

The second validation case for the BISON pump model is a generator load rejection with bypass valve opening test, performed on a Hamaoka Unit 5 (Reference 5). A generator load rejection initiates a fast closure of the Turbine Control Valves (TCVs). The closure of the TCVs initiates a reactor scram and a trip of four RIPs. As in the previous case, the flow through the tripped RIPs is negative and therefore outside the first quadrant of the pump characteristics diagram.

This transient is simulated using the BISON code with the recirculation pump model described Section 2.2. The BISON simulation was compared to experimental data in Figures 3 and 4 in Appendix A. As can be observed, the calculated core flow is in very good agreement with the test data, which proves the validity of the recirculation pump model implementation in the BISON code.

3 ADDITIONAL QUALIFICATION OF BISON MODELS

The BISON code is currently used in the United States for licensing evaluations of reload fuel and other plant changes requiring mainly limiting transient evaluation. However for evaluating all transients required for a first core transient analysis application some additional model description and qualifications are needed. [

]^{a,c}

In addition, the scram system design in the ABWR is different as compared to the previous BWRs. An advanced control rod insertion model will allow Westinghouse to simulate the control rod insertion as function of time to more accurately simulate the scram system performance.

It should be noted that these additional models are already used in licensing basis analyses in Europe, but have not been submitted to the U.S. NRC until now for review and approval.

3.1 ADVANCED CONTROL ROD HYDRAULIC INSERTION MODEL

3.1.1 Purpose

The purpose of this section is to provide a description and qualification of the advanced control rod hydraulic insertion model and to demonstrate the capability of the model to predict control rod insertion during scram. The latter will be shown by comparisons to measurements from plant startup tests and plant events.

3.1.2 Description of Model

3.1.2.1 Overview

The Westinghouse advanced control rod hydraulic insertion model is used for simulations of the control rod insertion times during a hydraulic insertion (scram). The model includes modelling of the gas tanks, water tanks, scram valves, control rods and piping within the control rod drive system as shown in Figure 3-1. Given input of these components' physical properties the model simulates a scram by calculating how [

]^{a,c}

The advanced control rod hydraulic insertion model is part of the Westinghouse 1D transient code BISON (Reference 1). The [ ]^{a,c} calculated by BISON is used by the advanced control rod hydraulic insertion model. The [

]^{a,c} is used to accurately determine the control rod hydraulic insertion time.

In the sections below the different parts of the advanced control rod hydraulic insertion model are described.

3.1.2.2 Model for Simulating Scram for Plants with ABWR Design

The calculation model for scram systems with the scram valves downstream of the water tanks (ABWR design) are illustrated by Figure 3-1.

The model calculates the control rod hydraulic insertion time by the [ ]a,c from the scram system. The [ ]a,c in the system is determined by [ ]a,c in the different parts of the system in the following way: a,c

[ ]

Each of these parts of the model is described in the sections below.

a,c

[ ]

Figure 3-1 Advanced Control Rod Hydraulic Insertion Model for ABWR

3.1.2.3 Opening of the Scram Valve

The scram valve in the water line is simulated by a restriction whose relative opening area during the opening phase is increased from 0 to 1 (full pipe area). [ ]a,c The relative opening area is described as:

a,c

[ ] Equation 3-1

For a restriction in the line with a relative opening A_{rel}, a pressure drop applies:

$$\Delta p = VALVE \cdot G_2^{\ 2} \qquad \text{Equation 3-2}$$

where the VALVE factor is defined as

a,c

[ ] Equation 3-3

For Equation 3-3 the assumption $A_{rel} > 0$ is made. Equation 3-3 then provides the scram valves' contribution to the pressure drop in the line. For a closed valve the factor VALVE is infinite, the flow G_2 is set to zero. For a fully opened valve, VALVE = 0.

3.1.2.4 Changes in the Gas Tank

When the scram valve is opened there will be a mass flow in the system. When the mass flow G_1 leaves the gas tank, pressure and temperature in the tank are changed. The temperature at the walls of the gas tank is presumed to be constant T_{10}. The temperature of the gas is T_1, with an initial value of T_{10}. The heat exchange between the walls and gas is included in the model (see Equation 3-6). Subsequently, there will be the following mass and energy balance for the gas tank:

$$\frac{dM_1}{dt} = -G_1 \qquad \text{Equation 3-4}$$

$$q_1 - G_1 \cdot h_1 = \frac{d}{dt}\left(M_1 \cdot u_1\right) \qquad \text{Equation 3-5}$$

Heat transfer is depicted as:

$$q_1 = \alpha_1 \cdot A_{w1} \cdot \left(T_{10} - T_1\right) \qquad \text{Equation 3-6}$$

The combination of Equation 3-4 through Equation 3-6 gives:

$$\frac{dT_1}{dt} = \frac{1}{M_1} \cdot \left(\frac{\kappa \cdot \alpha_1 \cdot A_{w1} \cdot \left(T_{10} - T_1\right)}{c_p} - \left(\kappa - 1\right) \cdot G_1 \cdot T_1 \right) \qquad \text{Equation 3-7}$$

Thus, the condition in the gas tank is described by differential Equation 3-4 and Equation 3-7.

3.1.2.5 Flow Between Gas Tank and Water Tank

The gas flow G_1 between the gas tank and the water tank is described according to the following. The pressure difference between the two tanks is:

$$dp_{12} = p_1 - p_2 \qquad \text{Equation 3-8}$$

The relationship between flow and pressure difference is expressed as:

a,c

[ ] Equation 3-9

An extra linear term in [

]a,c

3.1.2.6 Changes in the Water Tank

In the water tank there will be a gas volume and a water volume that both will change when the scram valve is opened and scram is initiated. The gas volume V_2 has a pressure p_2, and the following mass and energy balances apply respectively:

$$\frac{dM_2}{dt} = G_1 \qquad \text{Equation 3-10}$$

$$q_1 + G_1 \cdot h_G - p_2 \cdot \frac{dV_2}{dt} = \frac{d}{dt}\left(M_2 \cdot u_2\right) \qquad \text{Equation 3-11}$$

Where h_G is the stagnation enthalpy for the gas flow G_1. For $G_1 \geq 0$ $h_G = h_1$, and for $G_1 < 0$ $h_G = h_2$.

The equation of state for the gas is

$$\frac{p_2}{\rho_g} = R \cdot T_2 \qquad \text{Equation 3-12}$$

The initial temperature of the gas in the water tank is T_{20}. Furthermore, the following relationships apply

$$V_2 = V_{23} - V_3 \qquad \text{Equation 3-13}$$

$$p_2 = \frac{M_2 \cdot R \cdot T_2}{V_2} \qquad \text{Equation 3-14}$$

The heat transferring surface is calculated as if the gas volume has a spherical shape. This gives

$$V_2 = \frac{4}{3} \cdot \pi \cdot r^3 \qquad \text{Equation 3-15}$$

$$A_{w2} = 4 \cdot \pi \cdot r^2 \qquad \text{Equation 3-16}$$

which gives

$$A_{w2} = 4\pi \cdot \left(\frac{V_2 \cdot 3}{4 \cdot \pi}\right)^{2/3} \approx 5 \cdot V_2^{2/3} \qquad \text{Equation 3-17}$$

Heat flow is depicted as

$$q_2 = \alpha_2 \cdot A_{w2} \cdot (T_{20} - T_2) \qquad \text{Equation 3-18}$$

The stagnation temperature of the G_1 flow is written as

$$T_G = \frac{h_G}{c_p} \qquad \text{Equation 3-19}$$

The equations above give

$$\frac{dT_2}{dt} = \frac{1}{M_2} \cdot \left(\frac{5 \cdot \alpha_2 \cdot \kappa}{c_p} \cdot V_2^{2/3} \cdot (T_{20} - T_2) + G_1 \cdot (\kappa \cdot T_G - T_2) + \frac{\kappa \cdot p_2}{c_p} \cdot \frac{dV_3}{dt} \right) \qquad \text{Equation 3-20}$$

Thus, the condition in the gas tank is described by differential Equation 3-10 and Equation 3-20.

3.1.2.7 Flow from the Water Tank

The water flow G_2 from the water tank runs out in a main line and is distributed in branch lines, one for each control rod. For the flow in these lines [

]a,c The impulse equation for the water flow from the water tank to the rotary actuator can be written as:

a,c

[ ]

Equation 3-21

The pressure difference across the plunger is:

$$\Delta p_{45} = p_4 - p_5 - \rho_2 \cdot g \cdot (HP_5 - HP_4) \qquad \text{Equation 3-22}$$

Equation of motion for the rotary actuator (moving parts):

$$\Delta p_{45} \cdot A_4 - M_{don} \cdot g \cdot \left(1 - \frac{\rho_2}{\rho_s}\right) - F_R = M_{don} \cdot \alpha \cdot \frac{dw}{dt} \qquad \text{Equation 3-23}$$

Please observe that the second term in Equation 3-23 represents the "apparent weight" of the actuator in the water.

Equation 3-21 to Equation 3-23 give the following expression for the water flow G_2 from the water tank:

a,c

[ ]

Equation 3-24

In the equation above a term [ ]a,c The equation applies when the actuator is in motion.

If the effects of acceleration are disregarded, the pressure drop across the actuator (and the leakage area) is:

$$\Delta p_{45} = \frac{M_{don} \cdot g \cdot \left(1 - \frac{\rho_2}{\rho_s}\right) + F_R}{A_4} \qquad \text{Equation 3-25}$$

Before the actuators start to move, the entire flow in the branch lines G_3 moves through the leakage area A_{41}, i.e.

$$\Delta p_{45} = \frac{1}{2\rho_2} \cdot \left(\frac{G_3}{A_{41}}\right)^2 \qquad \text{Equation 3-26}$$

Equation 3-24 can the be rewritten to

a,c

[ ]

Equation 3-27

For Δp_{45} the smallest of the values should be selected according to Equation 3-25 and Equation 3-26. The equation then applies until the actuators are fully inserted, after which the following applies:

$$\frac{dG_2}{dt} = 0 \qquad \text{Equation 3-28}$$

and

$$\Delta p_{45} = p_2 - p_5 + \rho_2 \cdot g \cdot (HP_3 - HP_5) \qquad \text{Equation 3-29}$$

3.1.2.8 Flow in the Branch Lines

The flow G_3 in the branch lines is:

$$G_3 = \frac{G_2}{N_{don}} \qquad \text{Equation 3-30}$$

The leakage flow G_{41} (per actuator) is :

$$G_{41} = A_{41} \cdot \sqrt{2 \cdot \rho_2 \cdot \Delta p_{45}} \qquad \text{Equation 3-31}$$

3.1.2.9 Movement of the Control Rods

The velocity of the actuator is:

$$w = \frac{G_3 - G_{41}}{\rho_2 \cdot A_4} \qquad \text{Equation 3-32}$$

Finally, the position of the control rod is acquired from:

$$\frac{dx}{dt} = w \qquad \text{Equation 3-33}$$

The remaining volume of water in the water tank V_3 is obtained through integration of the outflow G_2, i.e.

$$\frac{dV_3}{dt} = \frac{G_2}{r_2} \qquad \text{Equation 3-34}$$

3.1.2.10 Water Inflow to the Reactor Pressure Vessel

During the hydraulic control rod insertion, there is a volume change in the water tank due to the water that is flowing to the core's bypass.

3.1.2.11 Hydraulic Brake

A hydraulic brake can be modeled in the end phase of the control rod hydraulic insertion. If there is a hydraulic brake in the scram system the actuator velocity is reduced during a set braking distance.

3.1.2.12 Initial insertion of control rods

In the model there is an option to prescribe that a number of control rods are already inserted into the core at the beginning of the control rod insertion. This is performed by prescribing that a number of actuators, N_{don1}, are extracted from the total N_{don} actuators in the group. The flow G_2, see Equation 3-27, will then be divided into two components according to:

$$G_2 = G_{21} + G_{22} \qquad \text{Equation 3-35}$$

where G_{21} is going to the N_{don1} extracted actuators and G_{22} is going to the $N_{don2} = N_{don} - N_{don1}$ non-extracted actuators. The flow for the extracted actuators will be:

$$\frac{dG_{21}}{dt} = \frac{1}{\frac{L_3}{A_3} + \frac{L_{32}}{N_{don1} \cdot A_{32}} + \frac{M_{don} \cdot \alpha}{\rho_2 \cdot A_4^{\,2} \cdot N_{don1}}} \cdot \{p_2 - p_5 - p_{br} + \rho_2 \cdot g \cdot (HP_3 - HP_5) - \Delta p_{45} - G_2^{\,2}\left(\frac{\xi_3}{2\rho_2 \cdot A_3^{\,2}} + VALVE\right) - G_{21}^{\,2} \cdot \frac{\xi_{32}}{2\rho_2 \cdot (A_{32} \cdot N_{don1})^2}\}$$

Equation 3-36

For the non-extracted N_{don} actuators (if there are any) analogously the following will apply

$$\frac{dG_{22}}{dt} = \frac{1}{\frac{L_3}{A_3} + \frac{L_{32}}{N_{don2} \cdot A_{32}} + \frac{M_{don} \cdot \alpha}{\rho_2 \cdot A_4^{\,2} \cdot N_{don2}}} \cdot \{p_2 - p_5 + \rho_2 \cdot g \cdot (HP_3 - HP_5) - G_2^{\,2} \cdot \left(\frac{\xi_3}{2\rho_2 \cdot A_3^{\,2}} + VALVE\right) - \frac{1}{2\rho_2} \cdot \frac{1}{(N_{don2} \cdot (A_{41} + A_{42}))^2} + G_{22}^{\,2} \frac{1}{(N_{don2} \cdot A_{32})^2}\}$$

Equation 3-37

3.1.3 Verification of model

In the sections below the verifications for the reactors [ ]^{a,c} and [ ]^{a,c} are shown.

3.1.3.1 Verification of the Model with Data from [ ]^{a,c}

[ ]^{a,c} is a BWR reactor of ASEA-ATOM design. The reactor is equipped with internal recirculation pumps and the rated thermal power is 1170 MW_e.

The 169 control rods in the reactor are divided into 18 groups with 8,9, or 10 rods per group. Each control rod group is connected to a hydraulic control unit that provides the hydraulic power required for a scram. Each hydraulic control unit contains a nitrogen tank, a water tank and the necessary valves and components to scram a group of control rods. The scram valve is situated between the gas tank and the water tank, which means that only the gas tank is held at high pressures during normal operation.

The advanced control rod hydraulic insertion model for [ ]^{a,c} has been verified against measurements of control rod hydraulic insertion from [ ]^{a,c} The tests have been performed at different reactor dome pressures and different pressures in the gas tanks. [

]^{a,b,c}

The measurements and the simulations with the advanced control rod hydraulic insertion model are shown in Figure 3-2. [

]^{a,c}

As can be seen from Figure 3-2 the model shows good agreement with measurements. This is especially true for the [

]^{a,c} The control rod groups containing more control rods have longer insertion times because the total weight of the control rods is larger in those groups and thus there is more mass to accelerate and insert.

a,b,c

[ ]

Figure 3-2 [ ]a,c Control Rod Hydraulic Insertion (SCRAM) Times

3.1.3.2 Verification of the Model with Data from [ ]a,c

[ ]a,c is an ABWR reactor. The reactor is equipped with internal recirculation pumps and the gross power is 1356 MW_e.

The 205 control rods in the reactor are divided into 102 groups with 2 rods per group and 1 group with only 1 control rod. Each control rod group is connected to a hydraulic control unit that provides the hydraulic power required for a scram. Each hydraulic control unit contains a nitrogen tank, a water tank and the necessary valves and components to scram a group of control rods. The scram valve is situated after the water tank, which means that both the gas tank and the water tank are held at high pressures during normal operation.

The advanced control rod hydraulic insertion model for [ ]a,c has been verified against measurements of control rod hydraulic insertion during [ ]a,c One group of control rods have been inserted at the time and the insertion time was recorded. The tests were performed at [

]a,b,c

The measurements and the simulations with the advanced control rod hydraulic insertion model are shown in Figure 3-3. As can be seen from Figure 3-3 the model shows good agreement with measurements. It should be noted that the agreement is very good for the [ ]^{a,c} that corresponds to nominal rated reactor [ ]^{a,c} At these [ ]^{a,c} the insertion times are important to predict well since they correspond to a situation with [ ]^{a,c}

a,b,c

[ ]

Figure 3-3 [ ]^{a,c} Control Rod Hydraulic Insertion (SCRAM) Times

3.1.4 Validation of Model

Validation of the Westinghouse advanced control rod hydraulic insertion model has been performed and documented for a control rod hydraulic insertion event in [ ]^{a,c}. Details on the event, including BISON calculation results for key parameters, are presented in the following sections.

3.1.4.1 [ ]^{a,c}

[ ]^{a,c} is a BWR reactor of ASEA-ATOM design. The reactor is equipped with external recirculation pumps and the rated thermal power is 1800 MW.

Description of the event

In [ ]^{a,c} an unplanned scram occurred in [ ]^{a,c} caused by an error in the turbine pressure regulator system originating from an error in the power supply. The error in the turbine pressure regulator system caused the turbine control valves to close from 100% capacity to 40% capacity in 5 seconds after which the valves rapidly closed completely. The turbine bypass valves remained closed

during the event. The closure of the turbine control valves caused the reactor dome pressure to increase, and the [ ]a,c The fast pressure increase in the reactor vessel triggered the reactor protection system which initiated a control rod hydraulic insertion (scram).

When the event was initiated the reactor was operating at nominal power and the recirculation flow was [ ]a,b,c.

[ ]a,c scram system

The scram system of [ ]a,c consists of 109 control rods divided into 17 groups. Of the 17 groups there are 3 different types of groups, as shown in Table 3-1. [ ]a,b,c

Table 3-1 Control Rod Groups in the [ ]a,c Scram System

Control rod group	No. of groups	No. of rods per group	Total no. of rods
1	2	5	10
2	6	6	36
3	9	7	63

Measurement data and comparison with BISON

Several parameters were recorded during the event, but the parameter of interest for this validation is the control rod insertion times. The insertion time was measured from scram signal to 100% insertion in the core. Table 3-2 shows the insertion times for the fastest, slowest and average rod for the three groups of control rods.

Table 3-2 Measured and Calculated Control Rod Insertion Times in [ ]a,c a,b,c

It should be noted that the number of control rods in a control rod group significantly effects the insertion time as well as their initial position.

The results show that simulations using the advanced control rod hydraulic insertion model agree well with measurement from the event, with the simulated insertion times [ ]a,c

3.1.5 Conclusions

The verification and validation presented demonstrates that the Westinghouse advanced control rod hydraulic insertion model is capable of modeling the hydraulic insertion of control rods. The predicted insertion times are in good agreement with measurements.

3.2 IMPROVED METHOD FOR CROSS-SECTION COLLAPSING

In the LTR for the BISON code (Appendix A to Reference 1) approved for licensing applications in 1989, three different methods were described to calculate coefficients of the polynomial equations for macroscopic cross-sections. The methods were "Single Fuel Type" (or Method A), "Multiple Fuel Types" (or Method B) and "Collapse from 3D Model" (or Method C).

The "Collapse from 3D Model" was the preferred method for limiting safety analyses. Based on results from the Peach Bottom 2 (PB2) turbine trip tests U.S. NRC found this acceptable. The U.S. NRC also found the other two methods acceptable for use in sensitivity studies and non-limiting events.

3.2.1 Purpose

After the introduction of the nodal code POLCA7 (Reference 7) in 2000, the "Multiple Fuel Types" cross-section method was further developed. This improved method utilizes detailed cross-section information from the 3D code POLCA7. With more detailed input this improved method is able to produce more accurate results when the cross-sections are collapsed to 1D for use in BISON. The further development of the "Multiple Fuel Types" method is presented below.

3.2.2 Description of the Improved Method

Currently, the "Multiple Fuel Types" cross-section collapsing method is used with the axial burnup or control rod density distribution search (as described in Section 4.6.3 in Reference 1) to match a user-specified power distribution and/or the k_{eff}. The main reason for the power distribution fitting is the simplified treatment of the density (or void) history dependence. The value of void history is considered constant, which introduces an axial power shape deviation. This deviation is compensated by the axial burnup or control rod density distribution search.

The improved collapsing method uses [ ]^{a,c} (obtained from a 3D nodal code) in each axial node and the [ ]^{a,c} for the axial power shape fitting procedure.

The following procedure is followed when generating the BISON kinetic model cross-sections.

- For all fuel elements in a 3D core, the cross-section polynomials are generated using the input from a 3D nodal code). These cross-section polynomials contain the data for all burnup steps and all density histories dependence data obtained from a 3D nodal code).

- [ ]a,c
- The 1D cross sections are used in BISON for transient analyses

[ ]a,c

3.2.3 Validation of Model

To validate the collapsing of the cross-sections is done correctly the results from POLCA7 and the improved method are compared.

3.2.3.1 Homogeneous Core

This section presents the validation of the improved "Multiple Fuel Types" cross-section collapsing method, when only one fuel assembly type is used in the reactor core (homogeneous core). BISON performs the steady state iteration using the burnup distribution defined in the input in order to obtain the axial power distribution.

A comparison of average axial power profile from POLCA7 and from the improved cross-section collapsing method is presented in Figure 3-4. As can be observed, the power profiles obtained by POLCA7 and BISON using the improved cross-section collapsing method are in very good agreement.

a,c

[ ]

Figure 3-4 Comparison of Homogeneous Core Normalized Axial Power Profile

A comparison of the reactivity change from a [ ]a,c change in recirculation flow obtained by 3D POLCA7 calculation and the BISON steady-state calculation with the cross-sections obtained using the improved "Multiple Fuel Type" method is performed. [ ]a,c

3.2.3.2 Mixed Core

The second validation case is performed on the ABWR reactor type model, where the reactor core is loaded with fuel assemblies of different types (mixed core). A comparison between the POLCA7 and the calculated axial power profiles is presented in Figure 3-5.

As can be observed, the power profiles obtained by POLCA7 and BISON using the improved cross-section collapsing method are in good agreement. Compared to the homogeneous core calculation, the difference between POLCA7 and the modified method is somewhat larger, which is assumed to be caused by the [ ]a,c

a,c

[ ]

Figure 3-5 Comparison of Heterogeneous Core Normalized Axial Power Profile

A comparison of the reactivity change from a [ ]a,c change in recirculation flow obtained by 3D POLCA7 calculation and the BISON steady-state calculation with the cross-sections obtained using the improved "Multiple Fuel Types" method is performed. The [

]a,c

3.2.3.3 Peach Bottom Test

During EOC2 in April 1977 three turbine trip tests, TT1, TT2 and TT3 were performed in the PB2 nuclear power station. PB2 is a BWR with a thermal power of 3293 MW and a steam dump capacity of 26.2% to the turbine condenser.

These transients have been described earlier as a part of the validation for BISON (Reference 1). Registrations were performed by means of station computer loggings and by instrumentation reading in the control room. During the transient, registrations were made with the plant's dynamic data acquisition system together with instrumentation installed specially for the tests. At each test 160 signals were registered and stored. The main process parameters from the tests are shown in Table 3-3 (Reference 1). The 3D reactor core model is created in POLCA7 and collapsed to 1D for use in BISON. The rest of the systems are modeled in the same way as in Reference 1.

Table 3-3 Peach Bottom 2 Main Process Parameters

Test	Power (%)	Core flow (%)	Scram limit, neutron flux (%)	Max APRM Q_{max}/Q_{in} (%)	Max steam dome pressure increase (MPa)
TT1	47.4	98.9	85	483	0.269
TT2	61.6	80.9	95	452	0.444
TT3	69.1	99.4	77	489	0.514

This section presents the validation results of the improved "Multiple Fuel Types" cross-section collapsing method. The BISON code is run [ ]^{a,c} or any other parameter is performed. As can be observed from Figure 3-6 to Figure 3-8 the initial axial power profile obtained by BISON agrees very well with the experimental data.

a,c

[ ]

Figure 3-6 Comparison of Normalized Axial Power Profile with Improved Cross-Section Collapsing Method for TT1

a,c

Figure 3-7 Comparison of Normalized Axial Power Profile with Improved Cross-Section Collapsing Method for TT2

a,c

Figure 3-8 Comparison of Normalized Axial Power Profile with Improved Cross-Section Collapsing Method for TT3

The calculated reactivity change caused by a [ ]a,c change in recirculation flow is compared to the 3D nodal code POLCA7. The results are shown in Table 3-4. [ ]a,c

Table 3-4 Reactivity Change Caused by a [ ]a,c Change in Recirculation Flow a,c

Figure 3-9 through Figure 3-14 show the transient APRM response at 0 to 4 seconds for TT1, TT2 and TT3 respectively. As a measure of energy release in the fuel bundles the time-integrated APRM signal can be used.

a,c

Figure 3-9 Comparison of APRM for TT1

a,c

Figure 3-10 Comparison of Integrated APRM for TT1

a,c

Figure 3-11 Comparison of APRM for TT2

a,c

Figure 3-12 Comparison of Integrated APRM for TT2

a,c

Figure 3-13 Comparison of APRM for TT3

a,c

[ ]

Figure 3-14 Comparison of Integrated APRM for TT3

Figure 3-9, Figure 3-11 and Figure 3-13 shows that BISON [ ]a,c the APRM transient response. Comparing the energy released in the fuel bundles, Figure 3-10, Figure 3-12 and Figure 3-14, it is shown that BISON [

]a,c

3.2.4 Conclusions

The improved "Multiple Fuel Types" method for BISON cross-section collapsing described above show that the BISON code can calculate the steady-state axial power profile accurately, without the need for any axial power shape fitting procedure.

The improved method validation included two cases, a core with one fuel type and one core with mixed fuel types. The obtained axial power profiles are compared to the ones obtained by the 3D nodal code POLCA7. The comparisons show good agreement.

Also a comparison of the PB2 turbine trip tests was performed using the improved "Multiple Fuel Types" method of BISON cross-section collapsing. The results show good agreement with the test data and [

]a,c

3.3 ASYNCHRONOUS PUMP MOTOR

The current approved BISON code (Reference 1) contains one recirculation flow control model which represents the entire pump. This calculates the pump head as function of pump flow and rotational speed. The pump speed may be prescribed by the user or calculated by the model. The model is an integrated part of the BISON code and it is not possible to control this model with control systems

In this section a new BISON model for the asynchronous pump motor is described. The new model is similar to the one mentioned above, except that only the asynchronous pump motor is modeled and the motor model can thus respond to signals from control system models.

3.3.1 Purpose

The introduction of the asynchronous pump motor model that can respond to signals from a control system makes it possible to have a more general control system for the recirculation flow by using a SAFIR control model (Reference 4). That means that the BISON asynchronous pump motor model can receive signals from a control system via a frequency converter model generated in SAFIR, and then calculate the speed of the pump.

3.3.2 Description of Model

A simplified model of the new BISON pump model is illustrated in Figure 3-15. The inputs to the BISON asynchronous motor model are a stator voltage (U_s) and a frequency (ω_s)of the magnetic field in the stator. This input may be generated by SAFIR or given as input directly by the user. The asynchronous motor model converts this to a torque on the pump and a rotational frequency of the rotor.

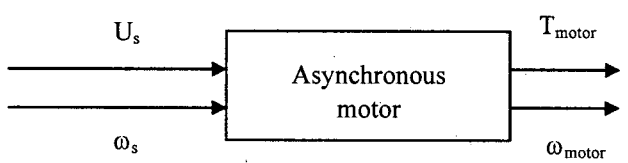

Figure 3-15 Block Diagram of the BISON Pump Model

However, the outputs are correlated as well since applying a larger torque implies an increase in rotational speed, according to the following equation:

$$\frac{d\omega_{motor}}{dt} = \frac{T_{motor} - T_{water} - T_{frict}}{I_{pump}} \qquad \text{Equation 3-39}$$

Where ω_{motor} is the rotational frequency of the motor and T_{motor} is the torque on the motor. I_{pump} is the moment of inertia of the pump. T_{water} and T_{frict} are torques arising from the water head and friction.

The BISON asynchronous motor model (where R_2 / SLIP represent the rotor) is simplified to the circuit seen in Figure 3-16:

a,c

[ ]

Figure 3-16 Equivalent Scheme For the BISON Model of the Asynchronous Motor

Where

a,c

[ ]

The asynchronous motor described is constructed to be connected to three phase electrical power. All derivations are for one phase where the three phases are performing with identical symmetry.

3.3.2.1 Deriving the Relationship Between Motor Torque and Stator Voltage

The power consumed by the pump per phase can be written as:

$$P = \frac{R_2 I_2^{\,2}}{k_s} \qquad \text{Equation 3-40}$$

where I_2 is the current going through R_2 and k_s is the slip factor, defined as

$$k_s = \frac{\omega_s - \omega_r}{\omega_r} \qquad \text{Equation 3-41}$$

where ω_s is the angular frequency of the magnetic field in the stator and ω_r is the angular frequency of the rotor, which is equal to ω_{motor} defined earlier. When no load is connected to an asynchronous motor the rotor frequency will be identical to the stator frequency and the slip factor is zero.

When using this method for calculating the power, the voltage over the circuit is defined with no phase difference (the current is defined complex with a reactive and an apparent part). An asynchronous motor is a big consumer of reactive power due to its requirement of magnetization current in the stator.

By using basic relations of electric circuitry and AC currents behavior, the current through the motor (R_2) can be written as the following function of the input voltage:

a,c

[ ]

Equation 3-42

where the impedances are defined in Table 3-5

Table 3-5 Defined Impedances in Figure 3-16

a,c

[ ]

The torque on the recirculation pump motor can be determined through the relation:

$$T_{motor} = \frac{P_m}{\omega_{motor}} \qquad \text{Equation 3-43}$$

where ω_{motor} is the motor angular frequency which is just $(1-k_s)\omega_s$. ω_s can be adjusted in different ways, usually by adjusting the frequency of the input voltage by using thyristors.

3.3.3 Validation of Model

The asynchronous pump motor has been validated through tests performed on the Hamaoka Unit 5 ABWR (Reference 5). This validation is done by varying the core flow and comparing plant response to predicted values. Hence, if the asynchronous motor is modeled incorrectly, the measured core flow will differ significantly from the model.

3.3.3.1 Recirculation Flow Control System Ramp Change

This test is performed by adding a -/+10% ramp change to the reactor power (load) setpoint. If the load setpoint is changed -10%, core flow is decreased in order to reduce the reactor power.

The reactor pressure decreases because of the power reduction, which generates voids in the reactor and an initial increase in vessel water level. After about 60 seconds, the reactor reaches another steady-state condition. As for the ramp change of plus disturbance, the transient shows almost an inverted response of the minus disturbance.

As can be observed in Figure 5 and Figure 6 in Appendix A, the calculated core flow is in satisfactory agreement with test data, implicitly proving the correctness of the asynchronous pump motor model in the BISON code.

3.3.3.2 All Main Steamline Isolation Valves Closure Test

This test simulates closure of all main steamline isolation valves (MSIVs). The MSIVs closure causes a pressure increase in the reactor and initiates a reactor scram trip via valve position signals to the reactor protection system. After the pressure exceeds the setpoint for the safety relief valves, the pressure increase is mitigated by opening these valves. Core flow initially decreases due to the RIPs runback due to the reactor scram. Reactor scram also causes a relatively large drop in vessel water level. Trip of four RIPs is initiated when the water level reaches the low water level setpoint.

As can be observed in Figure 7 and Figure 8 of Appendix A, the calculated core flow agrees with test data, implicitly proving the correctness of the asynchronous pump motor model in the BISON code.

3.3.3.3 Conclusions

The implementation of the models is validated against the experimental data obtained during the Hamaoka 5 reactor start-up tests. The comparison shows the calculated flow in satisfactory agreement with the test data, implicitly demonstrating the validity of the asynchronous pump motor model in the BISON code.

3.4 BISON/SAFIR INTERFACE FOR LEVEL MEASUREMENT

The BISON code (Reference 1) water level calculation is based on the water and steam mass balances in the upper plenum and in the downcomer. The first cell with water is assumed to contain the two-phase level. The two-phase level is derived from cell height in relation to the calculated steam and water volumes, this two-phase water level is not measured in a reactor. To be able to calculate the measured level, the use of the nozzle-component in BISON is described. The BISON nozzle component makes it possible to have a user defined position of evaluating pressure and temperature that is not limited to node limits. The BISON nozzle component also includes the effects from steam dryer pressure drop.

3.4.1 Purpose

The BISON nozzle component can be used to model water level measurement system for different types of BWR reactors. The models are based on the pressure difference between different nozzle nodes. This makes it possible to model several water level measurement systems for a plant, for example narrow range level and wide range level.

The BISON nozzle component is used to generate signals for nozzle pressure and nozzle temperature. The nozzles can be located anywhere in the nodes that are defined in BISON for steam-dome, bulk water and the downcomer. The position of the nozzle is defined by setting the elevation in relation to a reference zero level.

3.4.2 Description of Model

The RPV water level measurement model uses pressure differences from two nozzles in the RPV to calculate the water level. In BISON, the pressure is known at each node. To obtain the pressure at the nozzles, BISON performs a linear interpolation of the pressure from the adjacent node limits.

Assuming nozzle x is situated at height h_x between node n and $n+1$ at height h_n and h_{n+1}, all defined from an arbitrary reference level, the pressure at nozzle x can be written as

$$p(x) = p(n) + \frac{p(n+1) - p(n)}{h_{n+1} - h_n}(h_x - h_n) \qquad \text{Equation 3-44}$$

Figure 3-17 shows a sketch for a steam dryer and downcomer with resulting level changes. The pressure drop over the steam dryer can be expressed as a constant multiplied by the square of the steam flow through the steam dryer. This implies different levels, as can be seen in Figure 3-17.

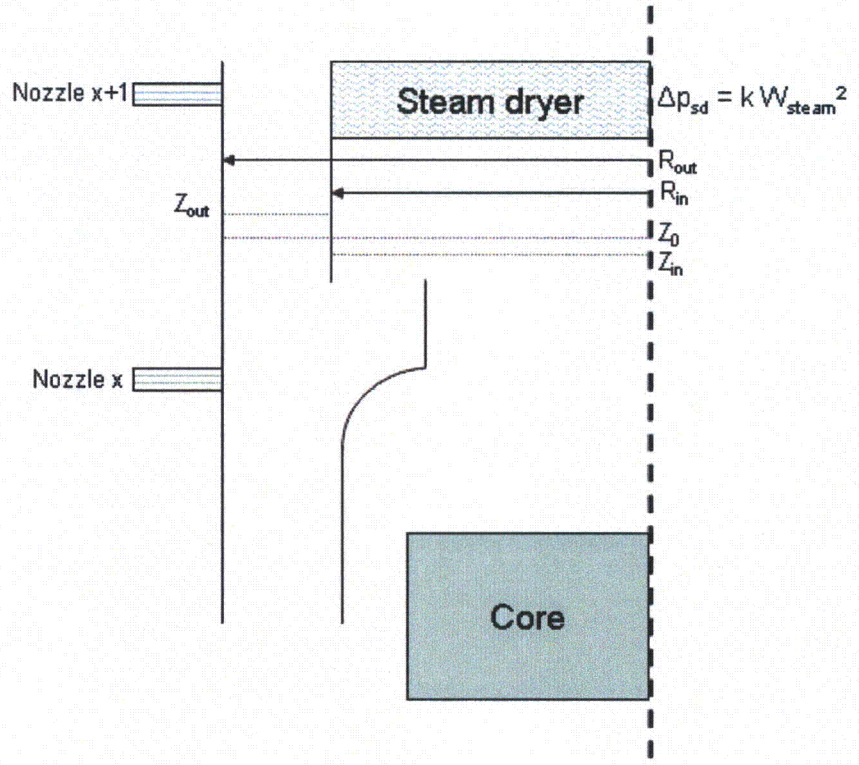

Figure 3-17 Representative Half Reactor Including the Stream Dryer in BISON

Z_0 is the non-modified BISON level,
Z_{out} is the adjusted level in the downcomer after the steam dryer correction, and
Z_{in} is the level in bulk water.

To obtain Z_{out}, two relations are used.

First, the water level change from the steam dryer pressure drop can be written as:

$$\Delta p_{sd} = \rho g \left(Z_{out} - Z_{in} \right) \qquad \text{Equation 3-45}$$

Second, the volume of suppressed water in the bulk water equals the volume of additional water in the steam annulus area. Hence,

$$\pi \left(R_{out}^{\ 2} - R_{in}^{\ 2} \right) \left(Z_{out} - Z_0 \right) = \pi R_{in}^{\ 2} \left(Z_0 - Z_{in} \right) \qquad \text{Equation 3-46}$$

Combining these two equations and solving for Z_{out} gives:

$$Z_{out} = Z_0 + \frac{R_{in}^{\ 2}}{R_{out}^{\ 2}} \frac{\Delta p_{sd}}{\rho g} \qquad \text{Equation 3-47}$$

When the nozzle is located below Z_{out}, the pressure in nozzle x is adjusted for the higher water level outside the dryer skirt. Hence,

$$p(x)_{sd,adj} = p(x) + \rho g\left(Z_{out} - Z_0\right) = p(x) + \frac{R_{in}^{\ 2}}{R_{out}^{\ 2}} \Delta p_{sd} \qquad \text{Equation 3-48}$$

These pressures at the nozzles described above can be used as input to model RPV water level measurement. The water level measurement system is needed for a more flexible non-limiting transient modeling.

3.4.3 Validation of Model

The RPV water level system is usually modeled using SAFIR. For those cases, the SAFIR model is validated for the first time application in connection with a License Amendment Request by comparing to plant data. An example to illustrate the process of validating such RPV water level system model is presented in the SAFIR Supplement, Section 6.2.2.4 of Reference 4.

3.5 STEAM DOME WATER SURFACE CONDENSATION MODEL

In the current approved BISON code (Reference 1) there are models describing the boiling mechanism (steam evaporation and condensation) using Solberg's model or Lellouche-Zolotar's model. These models describe the condensation in liquid due to changes in pressure/temperature or when subcooled water interacts with the steam environment. The steam condensation on the water surface of the bulk water is not accounted for. [

]a,c

3.5.1 Purpose

The purpose of the implementation of a model for water surface steam condensation is to better model the phenomena in the steam dome and in the bulk water.

Studying the Hamaoka 5 start-up tests there are some observations, which are summarized below:

- [

]a,c

To obtain better agreement between analysis and measurements, a model for steam condensation on the water surface was introduced. [

]a,c

3.5.2 Description of Model

The implemented model is a simple model with dependence of the subcooling of the water, the temperature difference between the water surface in comparison of the steam temperature, ΔT_{surf}. The dependence on subcooling is evaluated from the Hamaoka 5 start-up test measurements. The measurements results for LRWBP show that at about 70 seconds (Figure 4 in Appendix A) there is a slow decrease in the steam dome pressure. This slow decrease in pressure occurs when the water starts to subcool. [

]a,c

The applied model is a second degree polynomial versus the subcooling at the water surface, ΔT_{surf}, and the condensation C in kg/(sK) can be expressed as:

[ ]a,c Equation 3-49

Applying a [ ]a,c

3.5.3 Verification of Model

A verification of the fitting of condensation model was made. Figure 3-18 shows the [ ]a,c This is condensation versus ΔT_{surf} for test data and model result. The parameter [ ]a,c

a,c

Figure 3-18 Condensation Model Compared to Test Data

3.5.4 Validation of Model

The parameter [ ]a,c The Hamaoka 5 startup-test, as presented in Reference 5 is used. For the LRWBP test the results are as shown in Figure 3-19 below.

a,c

[ ]

Figure 3-19 Pressure (Pa) as a Function of Time (seconds) for a Load Rejection With Bypass Transient

In this case [ ]a,c predicts a pressure that agrees with the measured pressure [ ]a,c predict a slightly higher pressure of [ ]a,c This figure can be compared with the Figure 4 in Appendix A, which shows a comparison of BISON results and measurements data for LRWBP. As a comparison, [ ]a,c

For the MSIVC test reported in Reference 5, the result of a [ ]a,c is shown in Figure 3-20 below.

a,c

[ ]

Figure 3-20 Pressure (Pa) as a Function of Time (seconds) for a Main Steamline Isolation Valve Closure Transient

In this case [ ]a,c predicts the pressure [ ]a,c while the measured pressure is [ ]a,c predicts a pressure that agrees with the measured pressure [ ]a,c This figure can be compared with the Figure 8 in Appendix 1, which show a comparison of BISON results and measurements data for MSIVC.

3.5.5 Conclusions

The value of [ ]a,c is selected as the default value of the parameter.

The final correlation is now given as:

a,c

[ ] Equation 3-50

Using the condensation model gives an improved long term behavior of the pressure decrease and water level.

3.6 POST DRYOUT AND REWET MODEL

The currently approved BISON code (References 1 - 3) includes a method of calculating the Peak Cladding Temperature (PCT). The method described in Section 5.2.15 in Reference 6 describes how the time when dryout occurs is used as an input the PCT calculation. This is done by a combination of Bromley and Groeneveld correlations for post dryout heat transfer and no credit is taken for rewetting.

3.6.1 Purpose

This section contains a description and a validation of an improved cladding temperature model in BISON. The PCT model describes the heat transfer between the cladding and the coolant in the post dryout regime as well as the rewet quench velocity in the rewetting process.

3.6.2 Description of Model

The BISON model for cladding temperature mainly consists of three parts:

1. Determination of time for dryout and rewet

2. Determination of heat transfer between the cladding and the coolant in the post dryout regime

3. Determination of the rewetting velocity

The first part is fuel type dependent and utilizes the U.S. NRC approved CPR correlation for the fuel type in question to determine the time for dryout and start of the rewet process. The CPR correlation is approved during the licensing process for a new fuel type, and is not discussed any further in this topical.

The second part consists of a generic correlation that takes various geometrical data into account to describe the heat transfer between the cladding and the coolant in the post dryout regime. The heat transfer correlation for this purpose is described in Section 3.6.2.1.

Finally, the third part is a rewet correlation used to determine the rewet quench velocity. The correlation is a function of the temperature difference between the cladding and the water saturation temperature as shown in Section 3.6.2.2.

3.6.2.1 Post Dryout Heat Transfer Correlation

The objective of this section is to describe the heat transfer correlation utilized to determine the heat transfer between the cladding and the coolant in the post dryout regime. The modified Groeneveld heat transfer correlation is used for this purpose. The correlation consists of heat transfer terms due to radiation and partial and full film boiling.

The heat transfer coefficient due to radiation is:

$$HTC_{Rad} = \frac{T_{Wall}^4 - T_{Sat}^4}{T_{Wall} - T_{Sat}} * \sigma * \varepsilon \qquad \text{Equation 3-51}$$

where σ is the Stefan-Boltzmann's constant and ε is the emissivity of the surface and T is the temperature expressed in Kelvin.

The heat transfer coefficient due to partial and full film boiling is calculated using a combination of Bromley, Groeneveld and Dittus-Boelter heat transfer correlations. The two first correlations are utilized to determine the heat transfer from the cladding to the steam. In the transition boiling region, the heat transfer contribution from the cladding to the water drops is described by using the well-known Dittus-Boelter heat transfer correlations. Above the Leidenfrost temperature, the heat transfer regime switch over to one-phase steam. Thus, the contribution from Dittus-Boelter heat transfer correlation becomes zero when the cladding temperature reaches the Leidenfrost temperature.

Bromley heat transfer correlation:

$$A = \rho_G(\rho_F - \rho_G)^5 * g^5 * \lambda_G^3 * (T_{Wall} - T_{Sat})^3$$

$$B = 16.24 * \left(\frac{\sigma_F^4 * (h_{fg})^3 * Eta_G^5}{A}\right)^{1/11}$$

Equation 3-52

$$C = B^3 * g * \rho_G(\rho_F - \rho_G) * \frac{\Pr_G}{Eta_G^2}$$

$$HTC_{Br} = \left(C * \frac{h_{fg}}{Cp_G(T_{Wall} - T_{Sat})}\right)^{0.25} \frac{\lambda_G}{B} * 0.62$$

Groeneveld heat transfer correlation:

$$Y = 1 - 0.1 * \left(\frac{\rho_F}{\rho_G} - 1\right)^{0.4} * (1 - X)^{0.4}$$

$$PARAM = \mathrm{Re}_G * \left(X + \frac{\rho_G}{\rho_F} * (1 - X)\right)$$

$$HTC_{Gro} = \frac{\lambda_G}{D_h} * 0.052 * PARAM^{0.688} * \mathrm{Pr}_{GWall}^{1.26} * Y^{-1.06}$$ Equation 3-53

Dittus-Boelter heat transfer correlation:

$$HTC_{DB} = 0.023 * \frac{\lambda_F}{D_h} * \mathrm{Re}_F^{0.8} * \mathrm{Pr}_F^{0.4}$$ Equation 3-54

The modified Groeneveld heat transfer correlation is presented below. [

]a,c

Modified Groeneveld heat transfer correlation:

[ ]a,c

Equation 3-55

3.6.2.2 Rewet Model

[

]a,c

The correlation was derived using the experimental data obtained from the [ ]a,c The data that was used during the development of the rewet correlation and the rewet correlation itself are shown in Figure 3-21. As can be seen in the figure, a rewet quench velocity [ ]a,c

[ ]a,c

Equation 3-56

a,c

[ ]

Figure 3-21 Rewet Quench Velocity as a Function of Temperature Difference

3.6.3 Validation of Model

The BISON cladding temperature model has been validated against [ ]^{a,c} data for two different fuel types; [ ]^{a,c}

The predicted versus measured PCT increases are shown in Figure 3-22 for [ ]^{a,c} experiments. The mean error is [ ]^{a,c} The corresponding information for [ ]^{a,c} experiments are shown in Figure 3-24 through Figure 3-26 with a mean error of [ ]^{a,c}

a,c

[ ]

Figure 3-22 Predicted versus Measured Temperature Increases for [ ]^{a,c} Experiments

The predicted PCT, using the methodology applied for limiting transient evaluation, versus measured PCT increases are shown in Figure 3-23 for [ ]^{a,c} experiments. As it can be seen in the Figure 3-23 the PCT is conservatively predicted.

a,c

[ ]

Figure 3-23 Predicted versus Measured Temperature Increases for [ ]a,c Experiments, using conservative method for PCT calculation

a,c

[ ]

Figure 3-24. Predicted versus measured temperature increases for [ ]a,c

a,c

[ ]

Figure 3-25. Predicted versus measured temperature increases for [ ]a,c

a,c

[ ]

Figure 3-26. Predicted versus measured temperature increases for [ ]a,c

3.6.4 Conclusions

A description of the cladding temperature model is provided. The implementation of the model in the BISON transient code is validated against the experimental data obtained during the [ ]^{a,c} experiments. The comparison shows that the calculated PCT is in good agreement with experimental data with a [ ]^{a,c}

4 REFERENCES

1. RPA 90-90-P-A, "BISON – A One Dimensional Dynamic Analysis Code for Boiling Water Reactors, December 1991.

2. Westinghouse Report CENPD-292-P-A, "BISON - One Dimensional Dynamic Analysis Code for Boiling Water Reactors : Supplement 1 to Code Description and Qualification," July1996.

3. Westinghouse Report WCAP-16606-P-A, Rev 1, "Supplement 2 to BISON Topical Report RPA 90-90-P-A," January 2008.

4. Westinghouse Report WCAP-17079-P, "Supplement 3 to BISON Topical Report RPA 90-90-P-A SAFIR Control System Simulator," August 2009.

5. Proceedings of the 17th International Conference on Nuclear Engineering ICONE17, July 12-16, 2009, Brussels, BELGIUM ICONE17-75127, ABWR Start-up Test Analysis with Transient Code BISON.

6. Topical Report RPB 90-93-P-A, Rev. 0, "Boiling Water Reactor Emergency Core Cooling System Evaluation Model: Code Description and Qualification."

7. Westinghouse Report CENPD-390-P-A, Rev 0, "The Advanced PHOENIX and POLCA Codes for Nuclear Design of Boiling Water Reactors," December 2000.

APPENDIX A:
HAMAOKA 5 STARTUP TESTS

Figure 1 and 2 show a trip of three RIPs in Hamaoka 5 ABWR type reactor unit. The figures show a comparison of experimental data with computational results using the BISON code, as presented in Reference 5.

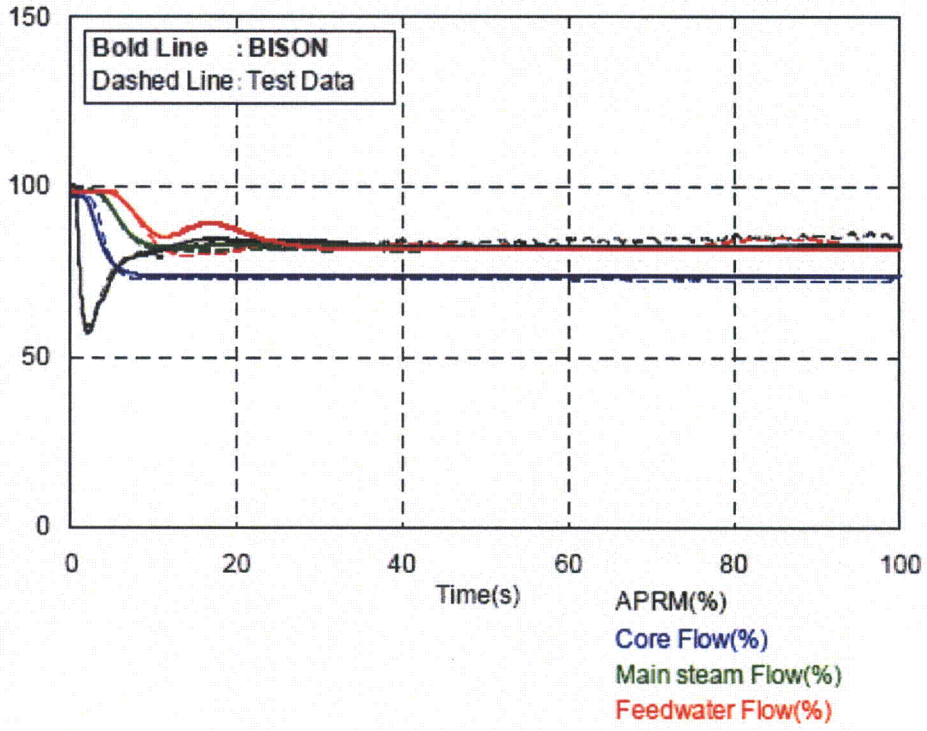

Figure 1 Trip of three out of ten RIP's test, main process parameters

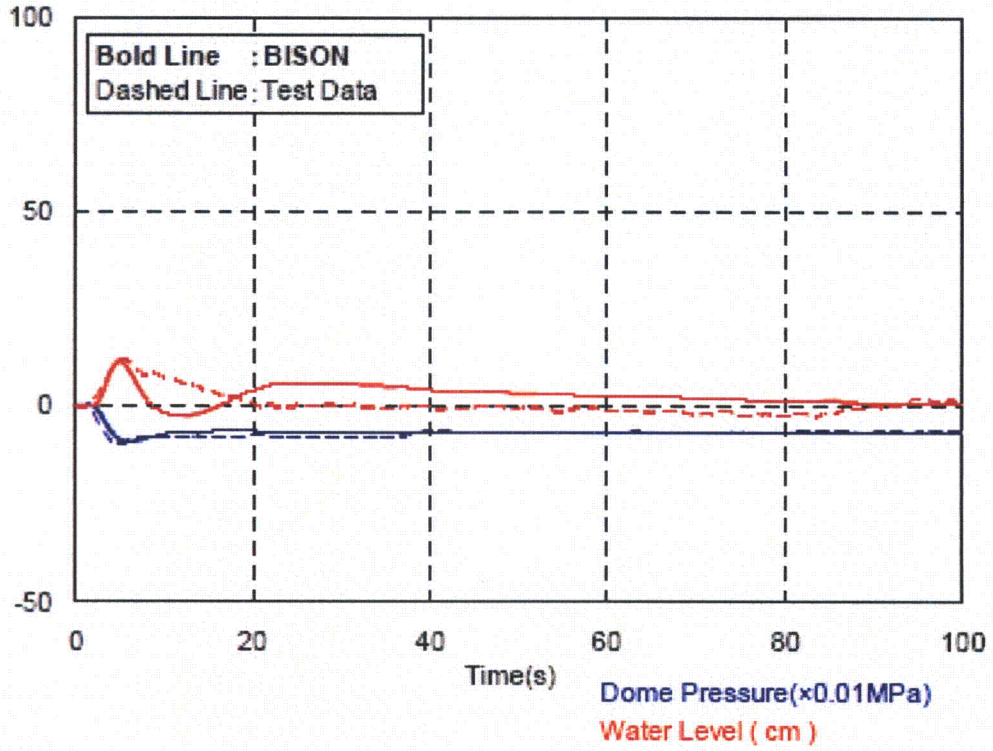

Figure 2 Trip of three out of ten RIP's test, changes of pressure and level compared to initial values

Figures 3 and 4 show a Generator Load Rejection Test in the Hamaoka 5 ABWR type reactor unit. The figures show a comparison of the experimental data with computational results using the BISON code, as presented in Reference 5.

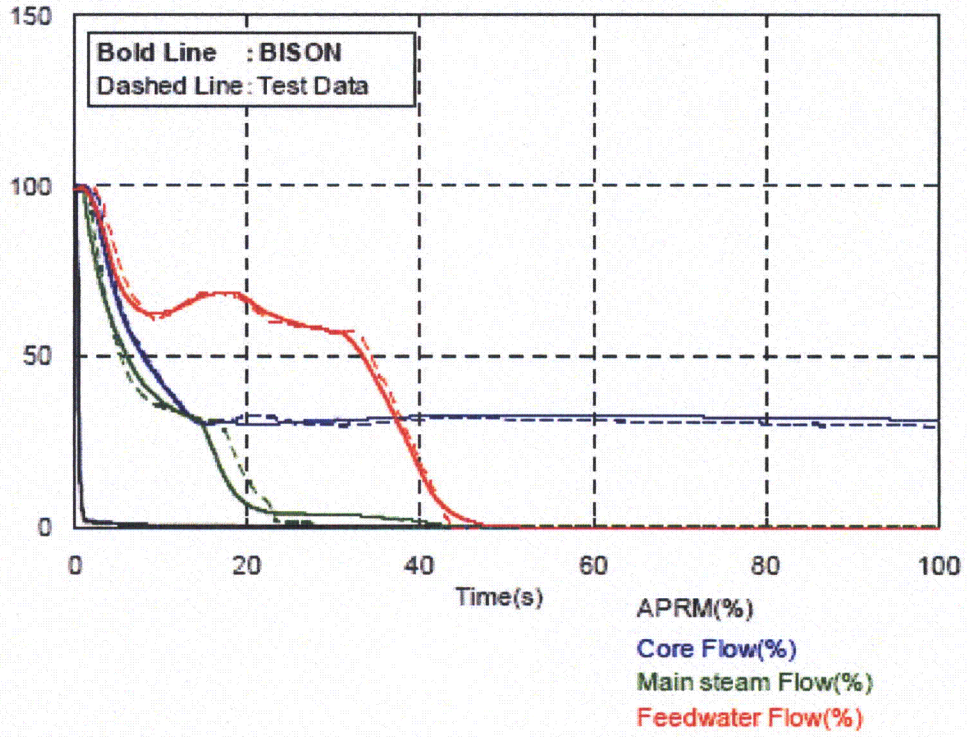

Figure 3 Generator load rejection test, main process parameters

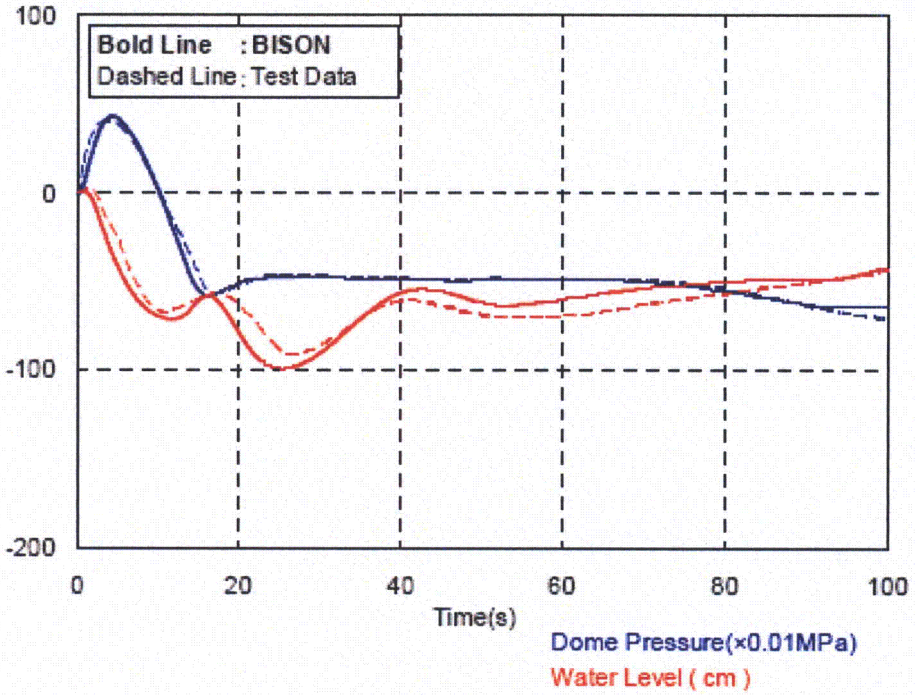

Figure 4 Generator load rejection test, changes of pressure and level compared to initial values

Load rejection is initiated whenever electrical grid disturbances occur which result in significant loss of electrical load on the generator. In this event, fast closure of the turbine control valves (TCVs) are activated by the power load unbalance relay. Fast closure of TCVs initiates a reactor scram and trip of four RIPs. The load rejection also causes a relatively large drop of water level due to scram initiation.

Figures 5 and 6 show a Recirculation control (ramp change) in the Hamaoka 5 ABWR type reactor unit. The figures show a comparison of experimental data with computational results using the BISON code, as presented in Reference 5.

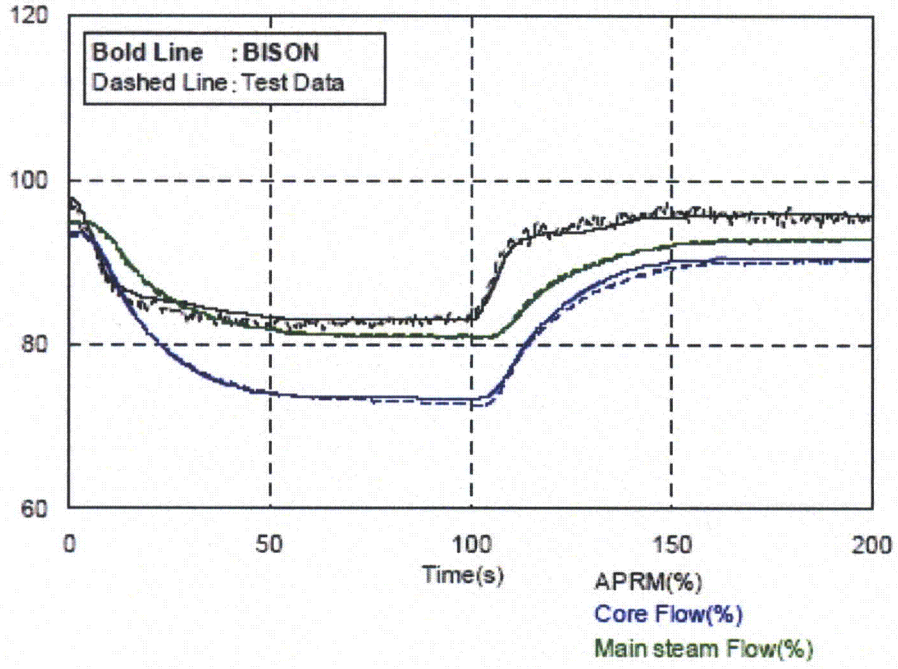

Figure 5 Recirculation control (ramp change) test, main process parameters

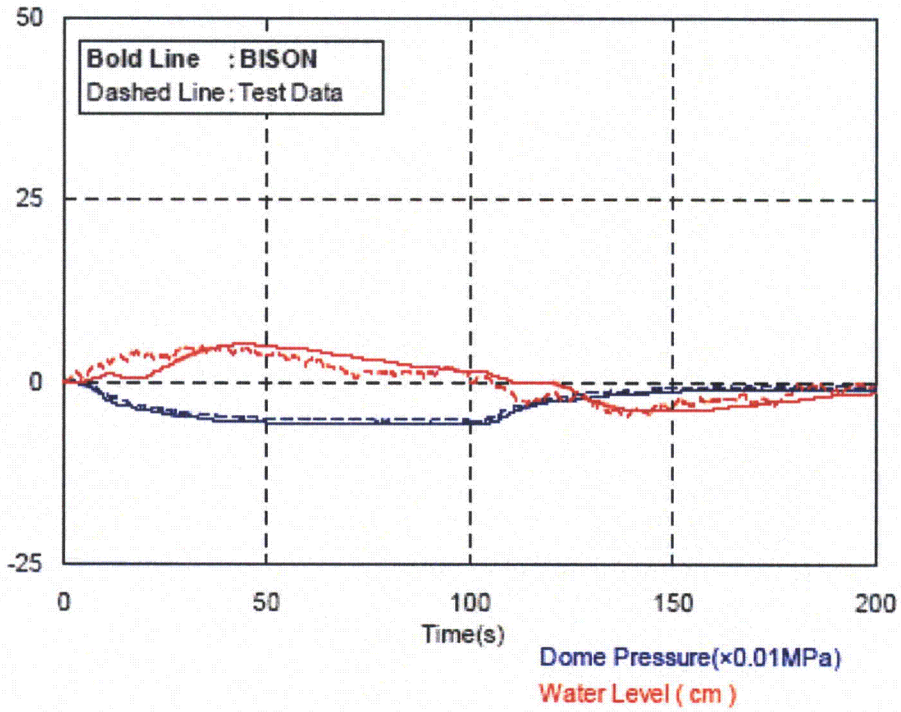

Figure 6 Recirculation control (ramp change) test, changes of pressure and level compared to initial values

This test is performed by addition of ramp input of -/+10% change of reactor power (load) setpoint. If load setpoint is changed -10%, core flow is decreased in order to reduce the reactor power.

The reactor pressure decreases because of the power reduction, which generates void in the reactor, and vessel water level initially increase. After about 60 seconds, the reactor has reached another stable steady-state condition. As for the ramp change of plus disturbance, the transient shows almost inverse response of the minus disturbance.

Figures 7 and 8 show an all MSIV closure test in Hamaoka 5 ABWR type reactor unit. The figures show a comparison of the experimental data with computational results using the BISON code, as presented in Reference 5.

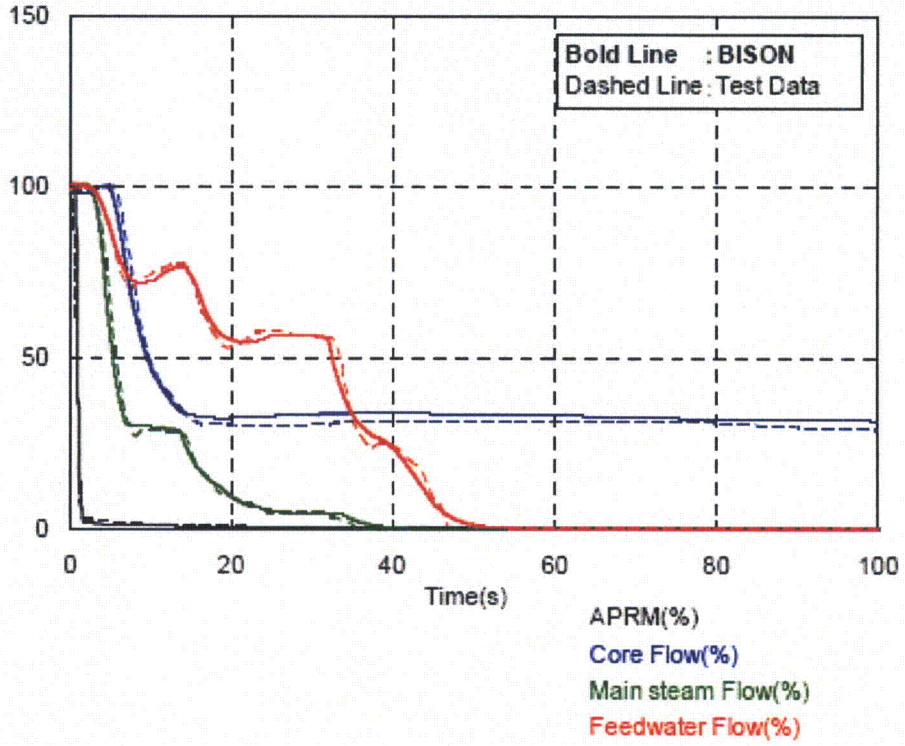

Figure 7 All MSIV closure test, main process parameters

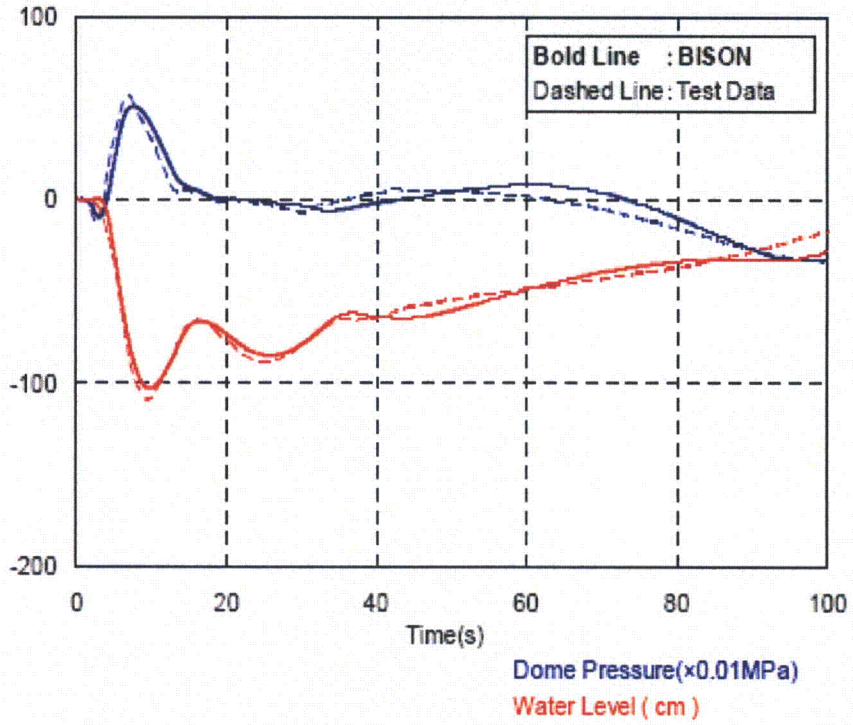

Figure 8 All MSIV closure test, changes of pressure and level compared to initial values

This test simulates closure of all main steamline isolation valves (MSIV). The MSIV closure causes pressure increase in the reactor and initiates a reactor scram trip via valve position signals to the reactor protection system. After the pressure exceeds the opening setpoint of the safety relief valves, pressure increase is mitigated by opening of the safety relief valves. Core flow initially decreases due to the RIPs runback according to the reactor scram. Reactor scram also causes a relatively large vessel water level drop and then water level reaches the low water level setpoint which initiates the trip of four RIPs.